Supplement of Atmos. Chem. Phys., 25, 11247–11260, 2025
https://doi.org/10.5194/acp-25-11247-2025-supplement
© Author(s) 2025. CC BY 4.0 License.

Atmospheric Chemistry and Physics
Open Access
EGU

Supplement of

Formation of chlorinated organic compounds from Cl atom-initiated reactions of aromatics and their detection in suburban Shanghai

Chuang Li et al.

Correspondence to: Lei Yao (lei_yao@fudan.edu.cn) and Lin Wang (lin_wang@fudan.edu.cn)

The copyright of individual parts of the supplement might differ from the article licence.

Section S1. Experimental setup in the laboratory.

A scheme of the flow tube set-up in our laboratory experiments is shown in Figure S1. Cl atoms were produced by photolysis of chlorine gases (Cl_2, Shanghai Wetry Standard Reference Gas Analytical Technology Co., LTD) using 350 nm UV lights (BL350 Linear T12, Feilo Sylvania International Group Co., LTD). Precursors (aromatics) were introduced into the flow tube using a custom-prepared gas cylinder generated through a low-pressure VOC loading system. Briefly, a clean stainless-steel cylinder was evacuated to ~10^{-2} mbar, after which a small amount of solid-phase aromatics precooled in liquid nitrogen was allowed to volatilize and fill the cylinder. The resulting pressure increase was monitored using a precision gauge, and once the target partial pressure was reached, the cylinder was sealed and then pressurized to 70 psi with high-purity nitrogen gas. To verify the precursor concentration, each gas cylinder was validated using a Vocus-PTR-LToF calibrated on the same day with certified commercial standards (Air Liquide Co., Ltd.). These VOCs included toluene, m-xylene, acetonitrile, acetaldehyde, methyl ethyl ketone (MEK), acetone, and acrylonitrile. VOCs were introduced into the flow system through a mass flow controller (MFC), with flow rates ranging from 0.05 to 10 sccm, depending on the specific compound and experimental conditions.

For each experiment, we first introduced the aromatic precursor after flushing the flow tube with zero air for over one hour. Once the concentration of aromatic precursor was stable, the chlorine gas was introduced into the flow tube. After 30 minutes, the UVA lamps were turned on and the reaction was allowed to proceed for 40-60 minutes.

Photolysis of VOC precursors and OVOC products is a typical issue that should be taken into account when evaluating the setting of flow tube experiments, especially in high UV light dose settings. In our experiments, the UV photon fluxes at 350nm was estimated to vary within the range of (1.9 - 3.7) $\times10^{14}$ photons cm^{-2} s^{-1} based on the distance between the light source and the flow tube. The light absorption wavelengths of aromatics primarily fall below 280 nm. For m-xylene, the absorption cross-section is 1.0×10^{-20} cm^2 at 280 ditunm (Keller-Rudek et al., 2013), and even lower at 350 nm, which suggests that its photolysis rate in our flow tube is likely less than 1.9×10^{-4} s^{-1}. Given that the rate constant for the reaction of m-xylene with Cl is 1.4×10^{-10} $molecule^{-1}$ cm^3 s^{-1} and the Cl concentration in the flow tube was determined to range from (3.3 - 5.5) $\times10^7$ molecule cm^{-3}, the Cl reaction rate for m-xylene was estimated to lie within (4.5 - 7.4) $\times10^{-3}$ s^{-1} (Wang et al., 2005). Therefore, the ratio of photolysis-to-Cl reaction was less than 0.01, indicating that photolysis of m-xylene was insignificant in the flow tube.

For stabilized products such as Cl-OOMs and non-Cl-OOMs, the relative significance of photolysis can also be estimated based on the photolysis rates of their proxies, since data for the exact compounds in our system are not available. The cross sections of organic molecules at 350 nm are approximately 7.1×10^{-18} cm^2 for Cl-OOMs (e.g., formylchloride oxide) and 1.2 $\times10^{-17}$ cm2 for non-Cl-OOMs (e.g., formaldehyde oxide) (Keller-Rudek et al., 2013). The photolysis quantum yields of multifunctional species are unlikely to be larger than those with only one carbonyl or one hydroxyl group, as discussed in previous studies (Peng et al., 2016; Peng and Jimenez, 2020), which are around 0.1. The UV photon fluxes at 350 nm ranged between (1.9 - 3.7) $\times10^{14}$ photons cm^{-2} s^{-1}, as mentioned earlier. Thus, an upper limit of the photolysis rates of Cl-OOMs was estimated to be 4.4×10^{-4} s^{-1} and 2.6×10^{-4} s^{-1} for non-Cl-OOMs. Hence, the ratio of photolysis to Cl reaction rates is estimated to be 0.06 for Cl-OOMs and 0.10 for non-Cl-OOMs, indicating the effect of the photolysis of VOC precursor and OVOC products on oxidation chemistry is minor.

Section S2. Setup of nitrate-CI-APi-LToF and Vocus-PTR-LToF, and their calibration in the field measurement.

As shown in Figure S3, in the charging region of the nitrate inlet, the sample flow stays in the center and is surrounded by a sheath air (zero air) carrying the nitrate ions that are electrostatically pushed into the sample flow. The sheath and sample flow rates were 20 L min^{-1} and 10 L min^{-1}, respectively. Sheath flow ensures that the sampling gas remains laminar, preventing the sample from contacting the walls of the sampler and thereby avoiding heterogeneous reactions. Under such conditions, the ion-molecule reaction time in the nitrate inlet was~200 ms. Ambient air was drawn into the nitrate inlet through a 1.2m long, 3/4-inch stainless steel tube, positioning the sampling point 1m from the wall. A flow of 0.8 L min^{-1} from the mixed flow passed through a critical orifice with a diameter of 0.3 mm to enter the APi-LTOF. During the field measurement, the nitrate-Cl-APi-LToF was calibrated using sulfuric acid, which initiates the production of sulfuric acid through the oxidation of SO_2 by OH (Kürten et al., 2012).

The Vocus-PTR-LToF utilized a 2 m-long Teflon tube with an outer diameter of 6.35 mm (1/4 inch) and an internal diameter of 3.97 mm (0.16 inch) as a sampling probe. A total flow rate of 5 L min^{-1} was maintained, with approximately 125 sccm directed into the Vocus PTR-TOF, while the remaining flow was managed by a blower. In the field measurement, the background check was performed twice every hour and VOC calibration once every hour. The programmed sample cycle lasted 1 h, which consisted of ambient sample measurements for 56 min, two background checks with one for 1 min and the other for 2 min, and a VOC calibration for 1 min.

Section S3. Applicability of flow tube experiments in atmospheric chemistry.

Flow tube experiments are highly relevant to atmospheric chemistry as the types of reaction products remain consistent even though their relative abundances may vary due to differences proportions in reaction pathways. This setup provides valuable insights into reaction mechanisms and product formation under controlled settings. It should be highlighted that, based on prior experience with OH oxidation flow tube experiments, the HO_2/RO_2 ratio observed in laboratory conditions differs from that in the actual atmosphere. While these discrepancies may influence the yields of stable products, they do not significantly impact the investigation of OOMs formation mechanisms (Baker et al., 2024; Wang et al., 2024). Additionally, 79% of the Cl-OOMs observed in the atmosphere were also detected in laboratory simulation experiments (refer to section 3.4), demonstrating similar formation mechanisms of Cl-OOMs between the laboratory results and ambient air. Moreover, it should be noted that dimer formation is favored in the flow tube compared to what would typically occur in the atmosphere, since the much-elevated RO2/HO2 ratios in the flow tube.

Section S4. The reactions of Cl-RO_2 and RO_2 with Cl, ClO, and Cl_2.

The reactions of Cl-RO_2 and RO_2 with Cl and ClO may also occur in chlorine-involved reactions. No current studies have investigated reaction rates between larger RO_2 species, such as the first-generation non-Cl-containing RO_2 radical (i.e., $C_8H_9O_2\cdot$) in Cl-m-xylene reaction, and Cl or ClO. Thus, the reported reaction rates of $CH_3O_2\cdot$ with Cl/ClO were adopted as surrogates: the reaction rate of RO_2 and Cl is estimated to be 1.60×10^{-10} cm^3 $molecule^{-1}$ s^{-1}, while the rate of RO_2 and ClO is 2.25×10^{-12} cm^3 $molecule^{-1}$ s^{-1}. (DeMore et al., 1997)

A PAM chemistry model (PAM_chem_v8), utilized widely in previous studies(Peng and Jimenez, 2020; Wang et al., 2024), was chosen with the latest updates to calculate radical profiles in our flow tube reactor. This model is based on a photochemical box model that includes the chemistry of photolysis of Cl_2 by the primary wavelengths at 350 nm and simplified VOC and RO_2 chemistry, but further reactions of the first-generation stabilized products and the second-generation organic radicals are not considered. The reactions and their corresponding kinetic coefficients utilized in this model are summarized in Table S6. In the model simulation, we assumed that half of the radicals/products from the reaction of Cl + m-xylene are RO_2, which subsequently react with Cl, ClO, RO_2, or undergo autoxidation, i.e., sequential isomerization and O_2 addition.

Figure S10 shows the concentration profiles of m-xylene, Cl, ClO, RO_2, and R'O_2 formed from the autooxidation of RO_2 in the flow tube reactor, as calculated using the PAM_chem_v8 model. The fate of RO_2, determined based on real-time concentrations and reaction rate constants, is shown in Figure S11. The RO_2 reaction channels stabilized by the 10th second and remain consistent until the reaction concludes. Throughout the entire reaction period in the flow tube, the fraction of the RO_2 + ClO reaction channel remains below 7%. It should be noted that the simulation results presented above are based on the assumption that the yield of RO_2 in the Cl + m-xylene reaction is 0.5. To evaluate the impact of the RO_2 yield on the experimental results, we conducted sensitivity tests with RO_2 yields set to be 0.3 and 1, and the proportion of the RO_2 + ClO channel was 9% and 5%, respectively. Assuming that the first-generation products are stable or react in similar rates, we integrated the product concentrations and found that the overall products proportion from the RO_2 + ClO channel is approximately 6%.

We arbitrarily set the fraction of the hydrogen abstraction pathway in the Cl-initiated reactions in the Cl-m-xylene system to be 86% (Huang et al., 2012). As a result, the overall contribution of the RO_2 + ClO channel to the product is estimated to be around 5%. On the other hand, it is widely agreed that the primary reaction channels for RO_2 + ClO involve the formation of ClOO + RO and ROCl + O_2 with a significant disagreement regarding their relative contributions (DeMore et al., 1997). Even if we use a 100% branching ratio for ROCl + O_2. the RO_2 + ClO pathway only represents about one-third of the Cl-OOMs formation. Therefore, RO_2 + ClO does not represent a primary formation pathway of Cl-OOMs.

Additionally, while RO can react with Cl_2, Platz et al. (1998) proposed via electronic structure calculations that the reaction of $C_6H_5O\cdot$ with Cl_2 to form C_6H_5OCl is a minor pathway (Platz et al., 1998). Based on their results, we conclude that the reaction of Cl_2 and RO is also not a significant contributor to Cl-OOMs formation in our experiments.

Section S5. Evaluating the role of OH chemistry under NOx-free conditions.

Although previous studies using modeling approaches have suggested that OH radicals are not formed in the Cl-atom-initiated oxidation of ethylbenzene under NOx-free conditions, OH can still be generated through H-abstraction from methyl groups by HO_2 (Bhattacharyya et al., 2023). Therefore, OH chemistry may also occur in our low-NOx experiments. To assess the potential influence of OH on product formation, we conducted additional experiments with the introduction of 20 ppm CO as an OH scavenger, following the setup described in Table 1 (Experiment 6). Product signals were measured using Vocus-PTR-LToF, I-CIMS, and nitrate-CI-APi-LToF.

Figure S12 displays the real-time signals of the first-generation products of Cl-initiated reaction and OH-initiated reaction and $C_8H_{11}ClO_{2\text{-}6}$ radicals. Upon CO (20 ppm) addition to ensure most of OH radicals were scavenged, the signal intensity of $C_8H_{12}O_5$ showed a noticeable decrease but did not fall to baseline (refer to Figure S12a). In contrast, the first-generation products from Cl-initiated reactions—namely C_8H_8O and $C_8H_{11}ClO_2$—were unaffected by the addition of CO. The signal intensity of another Cl-initiated product, $C_8H_{11}ClO_4$, decreased by approximately 50% upon CO addition. This indicates that its formation likely involves OH chemistry in addition to Cl reactions. These changes in stable products demonstrate the presence of OH chemistry even under low NOx conditions, suggesting that OH chemistry contributes to the formation of some of highly oxygenated Cl-OOM, thereby enhancing their yield.

Meanwhile, the $C_8H_{11}ClO_{1\text{-}6}$ radical signals (Figure S12b) remained unaffected by CO, confirming that these radicals originate exclusively from Cl-initiated chemistry. Collectively, these results affirm the contribution of OH to product formation without altering the main mechanistic conclusion that Cl-addition remains the dominant pathway for chlorinated radical and OOM formation in this system.

Table S1. Radicals detected by nitrate-CI-APi-LToF in the experiments of toluene, m-xylene, and 1,2,4-TMB with Cl atoms.

Toluene + Cl·	**Contributions to total identified radical signals in this group (%)**	**m-xylene + Cl·**	**Contributions to total identified radical signals in this group (%)**	**1,2,4-TMB + Cl·**	**Contributions to total identified radical signals in this group (%)**
$C_7H_8ClO_4NO_3^-$	10.5	$C_8H_{10}ClO_2I^-$	-	$C_9H_{12}ClO_4NO_3^-$	17.8
$C_7H_8ClO_5NO_3^-$	12.3	$C_8H_{10}ClO_3I^-$	-	$C_9H_{12}ClO_5NO_3^-$	20.5
$C_7H_8ClO_6NO_3^-$	24.1	$C_8H_{10}ClO_4NO_3^-$	3.5	$C_9H_{12}ClO_6NO_3^-$	23.0
$C_7H_8ClO_7NO_3^-$	10.5	$C_8H_{10}ClO_5NO_3^-$	17.1	$C_8H_{10}ClO_5NO_3^-$	12.7
$C_6H_6ClO_5NO_3^-$	8.1	$C_8H_{10}ClO_6NO_3^-$	27.4	$C_8H_{10}ClO_6NO_3^-$	17.3
$C_6H_6ClO_6NO_3^-$	9.9	$C_8H_{10}ClO_7NO_3^-$	14.1	$C_9H_{11}O_4NO_3^-$	3.2
$C_6H_6ClO_7NO_3^-$	8.0	$C_7H_8ClO_5NO_3^-$	5.4	$C_9H_{11}O_5NO_3^-$	5.4
$C_7H_7O_5NO_3^-$	3.6	$C_7H_8ClO_6NO_3^-$	8.8		
$C_7H_7O_6NO_3^-$	5.8	$C_7H_8ClO_7NO_3^-$	8.1		
$C_6H_5O_6NO_3^-$	7.2	$C_8H_9O_6NO_3^-$	10.2		
		$C_7H_7O_6NO_3^-$	5.3		

Table S2. Non-Cl-OOMs and Cl-OOMs detected by nitrate-CI-APi-LToF in the experiments of m-xylene with Cl atoms. Only the dominant products in the reaction of m-xylene with Cl atoms are shown. In the formulae, x represents the number of oxygens, ranging from 4 to 10.

Non-Cl-OOMs	Contributions to total identified product signals in the OOM group (%)	Cl-OOMs	Contributions to total identified product signals in the Cl-OOM group (%)
$C_8H_8O_x$	9.8	$C_8H_9ClO_x$	23.0
$C_8H_{10}O_x$	37.2	$C_8H_{11}ClO_x$	50.1
$C_8H_{12}O_x$	45.9	$C_8H_{13}ClO_x$	26.9
$C_8H_{14}O_x$	7.1		

Table S3. Average concentrations of ambient Cl-OOMs detected by nitrate-Cl-APi-LTOF between December 14th, 2022, and February 2nd, 2023, at the Dianshan Lake (DSL) Air Quality Monitoring Supersite in Shanghai, China.

Molecular formula	Concentration* (cm^{-3})	Molecular formula	Concentration * (cm^{-3})
$C_2H_2Cl_2O_2$	2.6×10^5	$C_7H_6NClO_3$	1.7×10^5
$C_2H_3ClO_2$	9.0×10^4	$C_7H_6N_3ClO_8$	5.4×10^4
$C_2H_9ClO_3$	7.2×10^4	$C_7H_7N_2ClO_8$	3.6×10^4
$C_3H_3ClO_2$	8.3×10^4	$C_7H_7N_2ClO_9$	2.6×10^4
$C_3H_3ClO_3$	5.1×10^4	$C_7H_7N_2ClO_{10}$	1.3×10^5
$C_4H_3ClO_3$	4.9×10^4	$C_7H_9ClO_{11}$	5.7×10^4
$C_4H_5ClO_3$	3.2×10^4	$C_7H_{11}N_2ClO_8$	5.7×10^4
$C_5H_5ClO_3$	1.2×10^5	$C_7H_{13}ClO_9$	5.5×10^4
$C_5H_5ClO_5$	9.4×10^4	$C_8H_7ClO_6$	4.4×10^5
$C_5H_6NClO_2$	6.3×10^4	$C_8H_7ClO_7$	8.2×10^4
$C_5H_6NClO_6$	1.3×10^5	$C_8H_{10}NClO_7$	2.1×10^4
$C_5H_6NClO_7$	7.0×10^4	$C_8H_{10}NClO_8$	3.4×10^4
$C_5H_7ClO_9$	7.4×10^4	$C_8H_{10}NClO_9$	5.1×10^4
$C_5H_7N_2ClO_4$	8.0×10^4	$C_8H_{12}NClO_7$	7.5×10^4
$C_5H_8NClO_5$	1.4×10^5	$C_8H_{12}Cl_2O$	1.1×10^5
$C_5H_9ClO_6$	1.2×10^5	C_9H_6NClO	4.4×10^5
$C_5H_9N_2ClO_7$	1.4×10^5	$C_9H_{11}ClO_{10}$	4.7×10^4
$C_6H_4NClO_3$	1.1×10^6	$C_9H_{15}ClO_8$	7.5×10^4
$C_6H_4NClO_4$	3.0×10^5	$C_{10}H_{12}NClO_3$	7.7×10^4
$C_6H_5N_2ClO_4$	2.2×10^4	$C_{11}H_6NClO_5$	8.0×10^4
$C_6H_5N_2ClO_6$	7.1×10^4	$C_{11}H_7ClO_5$	6.7×10^4
$C_6H_7N_2ClO_4$	6.4×10^4	$C_{11}H_8NClO_6$	2.7×10^4
$C_6H_9ClO_9$	5.3×10^4	$C_{11}H_{11}ClO_5$	8.7×10^4
$C_7H_5ClO_{11}$	4.2×10^4	$C_{14}H_{12}NClO_4$	3.6×10^4
$C_7H_5N_2ClO_5$	1.2×10^5	$C_{16}H_{11}ClO_4$	1.0×10^5
$C_7H_6NClO_5$	6.2×10^4		

***** Quantification of Cl-OOMs using the calibration factor of sulfuric acid may result in an uncertainty (± 50% as that of sulfuric acid) in the Cl-OOMs concentrations. The detection limit of the nitrate-Cl-APi-LTOF is 1.4×10^4 cm^{-3}.

Table S4. The adjacent peaks of the identified formulas in Table S3 and the reasons for their inconsistencies. Almost all NO was converted into NO_2 after the UV light was turned on.

Molecular formula	Other adjacent formulas	Error (ppm)	Unreasonable reasons
$C_2H_2Cl_2O_2(NO_3^-)$	$C_5Cl_2N_2O_2^-$	-14.1	Peak error is too large
$C_2H_3ClO_2(NO_3^-)$	$C_5O_6^-$	3.1	No hydrogen atom
$C_2H_9ClO_3(NO_3^-)$	$C_5H_6O_7^-$	2.7	Inappropriate hydrogen number
$C_3H_3ClO_2(NO_3^-)$	$C_6O_6^-$	2.9	No hydrogen atom
$C_3H_3ClO_3(NO_3^-)$	$C_6O_7^-$	2.65	No hydrogen atom
$C_4H_3ClO_3(NO_3^-)$	$C_7O_7^-$	2.49	No hydrogen atom
$C_4H_5ClO_3(NO_3^-)$	$C_7H_2O_7^-$	2.46	Inappropriate hydrogen number
$C_5H_5ClO_3(NO_3^-)$	$C_2Cl_2H_9N_3O_4^-$	-2.33	Inappropriate hydrogen number
	$C_8H_3NO_6^-$	2.33	Inappropriate hydrogen number
$C_5H_5ClO_5(NO_3^-)$	$C_2Cl_2H_8N_2O_7^-$	-2.01	Inappropriate hydrogen number
	$C_8H_2O_9^-$	2.01	Inappropriate hydrogen number
$C_5H_6NClO_2(NO_3^-)$	$C_2Cl_2H_9N_3O_4^-$	-2.33	Inappropriate hydrogen number
	$C_8H_3NO_6^-$	2.33	Inappropriate hydrogen number
$C_5H_6NClO_6(NO_3^-)$	$C_2Cl_2H_9N_3O_8^-$	-1.78	Inappropriate hydrogen number
	$C_8H_3NO_{10}^-$	1.78	Inappropriate hydrogen number
$C_5H_6NClO_7(NO_3^-)$	$C_2Cl_2H_9N_3O_9^-$	-1.68	Inappropriate hydrogen number
	$C_8H_3NO_{11}^-$	1.69	Inappropriate hydrogen number
$C_5H_7ClO_9(NO_3^-)$	$C_{15}Cl_2H_2N_4^-$	0.0844	Inappropriate hydrogen number
	$C_2Cl_2H_{10}N_2O_{11}^-$	-1.58	Inappropriate hydrogen number
	$C_8H_4O_{13}^-$	1.58	Too low C:O ratio
$C_5H_7N_2ClO_4(NO_3^-)$	$C_2Cl_2H_{10}N_4O_6^-$	-1.9	Inappropriate hydrogen number
	$C_8H_4N_2O_8^-$	1.9	Inappropriate hydrogen number
	$C_9N_6O_4^-$	-3.32	Inappropriate hydrogen number
$C_5H_8NClO_5(NO_3^-)$	$C_8H_5NO_9^-$	1.88	Inappropriate hydrogen number
	$C_2Cl_2H_{11}N_3O_7^-$	-1.88	Inappropriate hydrogen number
	$C_9HN_5O_5^-$	-3.28	Too high C:H ratio
$C_5H_9ClO_6(NO_3^-)$	$C_8H_6O_{10}^-$	1.86	Inappropriate hydrogen number
	$C_2Cl_2H_{12}N_2O_8^-$	-1.86	Inappropriate hydrogen number
	$C_9H_2N_4O_6^-$	-3.25	Too high C:H ratio
$C_5H_9N_2ClO_7(NO_3^-)$	$C_{23}NO^-$	-1.12	No hydrogen atom
	$C_2Cl_2H_{12}N_4O_9^-$	-1.59	Inappropriate hydrogen number
	$C_8H_6N_2O_{11}^-$	1.59	Inappropriate hydrogen number
$C_6H_4NClO_3(NO_3^-)$	$C_9HNO_7^-$	2.07	Too high C:H ratio
	$C_3Cl_2H_7N_3O_5^-$	-2.07	Inappropriate hydrogen number
	$CCl_2H_5N_6O_4^-$	3.64	Too high N: C ratio
$C_6H_4NClO_4(NO_3^-)$	$C_3Cl_2H_7N_3O_6^-$	-1.94	Inappropriate hydrogen number
	$C_9HNO_8^-$	1.94	Too high C:H ratio
	$CCl_2H_5N_6O_5^-$	3.41	Too high N: C ratio
$C_6H_5N_2ClO_4(NO_3^-)$	$C_3Cl_2H_8N_4O_6^-$	-1.83	Too high N: C ratio
	$C_9H_2N_2O_8^-$	1.83	Too high C:H ratio
	$C_2Cl_2H_{12}O_{10}^-$	3.2	Inappropriate hydrogen number

$C_6H_5N_2ClO_6(NO_3^-)$	$C_3Cl_2H_8N_4O_8$-	-1.63	Too high N: C ratio
	$C_9H_2N_2O_{10}^-$	1.63	Too high C:H ratio
	$C_2Cl_2H_{12}O_{12}^-$	2.85	Too low C:H ratio
$C_6H_7N_2ClO_4(NO_3^-)$	$C_3Cl_2H_{10}N_4O_6^-$	-1.82	Too high N: C ratio
	$C_9H_4N_2O_8^-$	1.82	Inappropriate hydrogen number
	$C_{10}N_6O_4^-$	-3.17	Inappropriate hydrogen number
$C_6H_9ClO_9(NO_3^-)$	$C_{16}Cl_2H_4N_4^-$	0.08	Too high C:H ratio
	$C_3Cl_2H_{12}N_2O_{11}^-$	-1.51	Too low C:H ratio
	$C_9H_6O_{13}^-$	1.51	Inappropriate hydrogen number
	$C_{19}ClHN_3O^-$	1.59	Too high C:H ratio
$C_7H_5ClO_{11}(NO_3^-)$	$C_{17}Cl_2N_4O_2^-$	0.07	No hydrogen atom
	$C_{10}H_2O_{15}^-$	1.35	Too high C:H ratio
	$C_4Cl_2H_8N_2O_{13}^-$	-1.35	Inappropriate hydrogen number
	$C_2Cl_2H_6N_5O_{12}^-$	2.36	Too high N: C ratio
$C_7H_5N_2ClO_5(NO_3^-)$	$C_{10}H_2N_2O_9^-$	1.66	Too high C:H ratio
	$C_4Cl_2H_8N_4O_7^-$	-1.66	Too high N: C ratio
	$C_3Cl_2H_{12}O_{11}^-$	2.89	Too low C:H ratio
$C_7H_6NClO_5(NO_3^-)$	$C_{10}H_3NO_9^-$	1.73	Too high C:H ratio
	$C_4Cl_2H_9N_3O_7^-$	-1.74	Inappropriate hydrogen number
	$C_2Cl_2H_7N_6O_6^-$	3.04	Too high N: C ratio
$C_7H_6NClO_3(NO_3^-)$	$C_{10}H_3NO_7^-$	1.96	Inappropriate hydrogen number
	$C_4Cl_2H_9N_3O_5^-$	-1.96	Inappropriate hydrogen number
	$C_2Cl_2H_7N_6O_4^-$	3.44	Too high N: C ratio
$C_7H_6N_3ClO_8(NO_3^-)$	$C_{18}Cl_2H_7O_4^-$	0.06	Too high C:H ratio
	$C_{10}H_3N_3O_{12}^-$	1.36	Too high C:H ratio
	$C_3Cl_2H_{13}NO_{14}^-$	2.38	Too low C:H ratio
$C_7H_7N_2ClO_8(NO_3^-)$	$C_{10}H_4N_2O_{12}^-$	1.42	Inappropriate hydrogen number
	$C_4Cl_2H_{10}N_4O_{10}^-$	-1.42	Too high N: C ratio
	$C_3Cl_2H_{14}O_{14}^-$	2.47	Too low C:H ratio
	$C_5ClH_5N_6O_{10}^-$	3.9	Too high N: C ratio
$C_7H_7N_2ClO_9(NO_3^-)$	$C_{17}Cl_2H_2N_6^-$	0.08	Too high C:H ratio
	$C_4Cl_2H_{10}N_4O_{11}^-$	-1.35	Too high N: C ratio
	$C_{10}H_4N_2O_{13}^-$	1.35	Too high C:H ratio
	$C_{11}N_6O_9^-$	-2.36	No hydrogen atom
$C_7H_7N_2ClO_{10}(NO_3^-)$	$C_{17}Cl_2H_2N_6O^-$	0.08	Too high C:H ratio
	$C_4Cl_2H_{10}N_4O_{12}^-$	-1.29	Too high N: C ratio
	$C_{10}H_4N_2O_{14}^-$	1.3	Too high C:H ratio
	$C_{22}ClHN_2O_3^-$	-2.21	Too high C:H ratio
$C_7H_9ClO_{11}(NO_3^-)$	$C_{17}Cl_2H_4N_4O_2^-$	0.08	Too high C:H ratio
	$C_{10}H_6O_{15}^-$	1.33	Inappropriate hydrogen number
	$C_4Cl_2H_{12}N_2O_{13}^-$	-1.33	Too low C:H ratio
	$C_{20}ClHN_3O_3^-$	1.4	Too high C:H ratio
	$C_{11}H_2N_4O_{11}^-$	-2.32	Too high C:H ratio
$C_7H_{11}N_2ClO_8(NO_3^-)$	$C_{25}H_2NO_2^-$	-0.98	Too high C:H ratio

	$C_{10}H_8N_2O_{12}^-$	1.4	Inappropriate hydrogen number
	$C_4Cl_2H_{14}N_4O_{10}^-$	-1.4	Too high N: C ratio
	$C_3Cl_2H_{18}O_{14}^-$	2.44	Too low C:H ratio
	$C_{11}H_4N_6O_8^-$	-2.44	Too high N number
$C_7H_{13}ClO_9(NO_3^-)$	$C_{17}Cl_2H_8N_4^-$	0.07	Too high C:H ratio
	$C_{10}H_{10}O_{13}^-$	1.44	Inappropriate hydrogen number
	$C_4Cl_2H_{16}N_2O_{11}^-$	-1.44	Too high C:H ratio
	$C_{11}H_6N_4O_9^-$	-2.52	Inappropriate hydrogen number
	$C_8ClH_9N_5O_8^-$	-3.96	Too high N number
$C_8H_7ClO_6(NO_3^-)$	$C_{11}H_4O_{10}^-$	1.65	Inappropriate hydrogen number
	$C_5Cl_2H_{10}N_2O_8^-$	-1.65	Inappropriate hydrogen number
	$C_{12}N_4O_6^-$	-2.87	No hydrogen atom
	$C_3Cl_2H_8N_5O_7^-$	2.89	Too high N: C ratio
$C_8H_7ClO_7(NO_3^-)$	$C_5Cl_2H_{10}N_2O_9^-$	-1.56	Inappropriate hydrogen number
	$C_{11}H_4O_{11}^-$	1.56	Inappropriate hydrogen number
	$C_{12}N_4O_7^-$	-2.66	No hydrogen atom
	$C_3Cl_2H_8N_5O_8^-$	-2.72	Too high N: C ratio
$C_8H_{10}NClO_7(NO_3^-)$	$C_5Cl_2H_{13}N_3O_9^-$	-1.48	Inappropriate hydrogen number
	$C_{11}H_7NO_{11}^-$	1.48	Inappropriate hydrogen number
	$C_{23}ClH_4N^-$	-2.52	Too high C:H ratio
	$C_3Cl_2H_{11}N_6O_8^-$	2.6	Too low C:H ratio
$C_8H_{10}NClO_8(NO_3^-)$	$C_{11}H_7NO_{12}^-$	1.41	Inappropriate hydrogen number
	$C_5Cl_2H_{13}N_3O_{10}^-$	-1.41	Too low C:H ratio
	$C_{23}ClH_4NO^-$	-2.41	Too high C:H ratio
	$C_{12}H_3N_5O_8^-$	-2.47	Too high C:H ratio
$C_8H_{10}NClO_9(NO_3^-)$	$C_{11}H_7NO_{13}^-$	1.35	Inappropriate hydrogen number
	$C_{12}H_3N_5O_9^-$	-2.36	Too high C:H ratio
	$C_9ClH_6N_6O_8^-$	-3.7	Too high N number
	$C_6ClH_8N_5O_{11}^-$	3.72	Inappropriate hydrogen number
$C_8H_{12}NClO_7(NO_3^-)$	$C_{11}H_9NO_{11}^-$	-1.4	Inappropriate hydrogen number
	$C_3Cl_2H_{13}N_6O_8^-$	0.92	Too low C:H ratio
	$C_6ClH_{10}N_5O_9^-$	2.4	Too high N: C ratio
	$C_{17}Cl_2H_{11}NO_2^-$	2.46	Inappropriate hydrogen number
$C_8H_{12}Cl_2O(NO_3^-)$	$C_{15}H_2N_3O_2^-$	-1.42	Too high C:H ratio
	$C_{11}ClH_9O_5^-$	1.9	Inappropriate hydrogen number
	$C_{12}ClH_5N_4O^-$	-3.32	Inappropriate hydrogen number
	$C_2H_{10}NO_{13}^-$	-3.42	Too low C:H ratio
$C_9H_6NClO(NO_3^-)$	$C_6Cl_2H_9N_3O_3^-$	-2.02	Inappropriate hydrogen number
	$C_{12}H_3NO_5^-$	2.02	Too high C:H ratio
	$C_4Cl_2H_7N_6O_2^-$	3.55	Too high N number
$C_9H_{11}ClO_{10}(NO_3^-)$	$C_{19}Cl_2H_6N_4O^-$	0.07	Too high C:H ratio
	$C_{12}H_8O_{14}^-$	1.3	Inappropriate hydrogen number
	$C_{24}ClH_5O_3^-$	2.28	Too high C:H ratio
	$C_{21}Cl_2H_8NO_2^-$	-3.5	Too high C:H ratio

$C_9H_{15}ClO_8(NO_3^-)$	$C_6Cl_2H_{18}N_2O_{10}^-$	-1.4	Too low C:H ratio
	$C_{12}H_{12}O_{12}^-$	1.4	Inappropriate hydrogen number
	$C_{24}ClH_9O^-$	-2.38	Too high C:H ratio
	$C_{13}H_8N_4O_8^-$	-2.44	Inappropriate hydrogen number
	$C_{10}ClH_{11}N_5O_7^-$	-3.84	Too high N number
$C_{10}H_{12}NClO_3(NO_3^-)$	$C_{13}H_9NO_7^-$	1.67	Inappropriate hydrogen number
	$C_7Cl_2H_{15}N_3O_5^-$	-1.67	Too low C:H ratio
	$C_5Cl_2H_{13}N_6O_4^-$	2.94	Too high N: C ratio
$C_{11}H_6NClO_5(NO_3^-)$	$C_{14}H_3NO_9^-$	1.48	Too low C:H ratio
	$C_8Cl_2H_9N_3O_7^-$	-1.48	Inappropriate hydrogen number
	$C_6Cl_2H_7N_6O_6^-$	2.6	Too high N: C ratio
$C_{11}H_7ClO_5(NO_3^-)$	$C_{14}H_4O_9^-$	-0.07	Too high C:H ratio
	$C_8Cl_2H_{10}N_2O_7^-$	-1.54	Inappropriate hydrogen number
	$C_6Cl_2H_8N_5O_6^-$	2.71	Too high N: C ratio
$C_{11}H_8NClO_6(NO_3^-)$	$C_{14}H_5NO_{10}^-$	1.4	Too high C:H ratio
	$C_8Cl_2H_{11}N_3O_8^-$	-1.4	Inappropriate hydrogen number
	$C_6Cl_2H_9N_6O_7^-$	2.47	Too high N: C ratio
	$C_9ClH_6N_5O_8^-$	3.87	Inappropriate hydrogen number
$C_{11}H_{11}ClO_5(NO_3^-)$	$C_8Cl_2H_{14}N_2O_7^-$	-1.52	Inappropriate hydrogen number
	$C_{14}H_8O_9^-$	1.52	Inappropriate hydrogen number
	$C_{15}H_4N_4O_5^-$	-2.66	Too high C:H ratio
	$C_6Cl_2H_{12}N_5O_6^-$	2.67	Too high N: C ratio
$C_{14}H_{12}NClO_4(NO_3^-)$	$C_3H_{11}N_6O_{14}^-$	-0.06	Too high N: C ratio
	$C_{11}Cl_2H_{15}N_3O_6^-$	-1.37	Inappropriate hydrogen number
	$C_{17}H_9NO_8^-$	1.37	Inappropriate hydrogen number
	$C_{18}H_5N_5O_4^-$	-2.39	Inappropriate hydrogen number
	$C_{12}ClH_{10}N_5O_6^-$	3.78	Too high N number
$C_{16}H_{11}ClO_4(NO_3^-)$	$C_5H_{10}N_5O_{14}^-$	-0.06	Too high N: C ratio
	$C_{13}Cl_2H_{14}N_2O_6^-$	-1.34	Inappropriate hydrogen number
	$C_2ClH_{13}N_6O_{13}^-$	-1.39	Inappropriate hydrogen number
	$C_{20}H_4N_4O_4^-$	-2.34	Too high C:H ratio
	$C_{11}Cl_2H_{12}N_5O_5^-$	2.35	Too high N number
	$C_4H_{14}NO_{18}^-$	3.62	Too high C:H ratio

Table S5. Toxicity prediction results for possible chemical structures of molecular formulae observed in the atmosphere in Shanghai.

No.	Molecular formula	SMILES	Half-life (Days (12-hour day; 1.5×10^6 OH/cm^3))	Bioconcentration factors (BCF) (log10_pred)	Oral rat pLD_{50} (-log10_pred_mol/kg)	pLD_{50} level*	Pred Developmental Toxicity**	Pred Mutagenicity **
1	$C_8H_{10}NClO_9$ (I)	Cl[C@@H]([C@]1(CO[N+]([O-])=O)C(OO)C=C2)[C@@]2(OO1)COO	0.16	1.55	2.29	4.0	0.88	0.32
2	$C_8H_{10}NClO_9$ (II)	O[C@@H]([C@]1(CO[N+]([O-])=O)C(OO)CC2=O)[C@@]2(OO1)CCl	0.29	0.70	2.31	4.0	0.92	0.71
3	$C_8H_{10}NClO_8$	Cl[C@@H]([C@]1(CO[N+]([O-])=O)C(OO)C=C2)[C@@]2(OO1)CO	0.16	1.28	2.55	3.0	0.87	0.47
4	$C_8H_{10}NClO_7$(I)	C[C@]1(OO2)[C@@H](Cl)[C@]2(CO[N+]([O-])=O)C(OO)C=C1	0.17	1.82	2.73	3.0	0.92	0.71
5	$C_8H_{10}NClO_7$(II)	C[C@]1(OO2)[C@@H](Cl)[C@]2(C)C3C(O[N+]([O-])=O)C1OO3	5.11	2.77	1.94	4.0	0.68	1.04
6	$C_8H_{12}Cl_2O$	OC1=CC=C(CCl)C=C1CCl	0.72	1.07	2.05	4.0	0.66	0.35
7	$C_7H_7N_2ClO_8$	Cl[C@@H]1[C@H](OO2)C(O[N+]([O-])=O)C=C[C@@]12CO[N+]([O-])=O	0.38	1.56	2.52	3.0	0.88	0.27
8	$C_7H_7N_2ClO_9$	Cl[C@@H]1[C@@](OO2)(O)C(O[N+]([O-])=O)C=C[C@@]12CO[N+]([O-])=O	0.36	1.14	1.99	4.0	1.05	0.18
9	$C_7H_7N_2ClO_{10}$	O[C@@H]([C@H]1OO2)[C@@]2(CO[N+]([O-])=O)C(O[N+]([O-])=O)C(Cl)C1=O	0.46	0.41	2.34	4.0	1.04	0.46
10	$C_9H_{15}ClO_8$ (I)	O[C@@H]1[C@@]2(C)C(OO)C(O)C(C)(OO)[C@]1(CCl)OO2	0.37	1.27	2.29	4.0	0.73	1.00
11	$C_9H_{15}ClO_8$ (II)	O[C@@H]1[C@@]2(CCl)C(OO)C(O)C(C)(OO)[C@]1(C)OO2	0.37	1.28	2.29	4.0	0.66	1.00

12	$C_9H_{15}ClO_8$ (III)	O[C@@H]1[C@@]2(C)C(OO)C(O)C(CCl)(OO)[C@]1(C)OO2	0.37	1.33	2.29	4.0	0.65	1.00
13	$C_7H_6NClO_5$	O=C1C=C[C@H]2[C@H]([N+]([O-])=O)[C@]1(CCl)OO2	0.20	0.89	1.70	4.0	0.46	0.67
14	$C_7H_9ClO_{11}$	O[C@]1(Cl)[C@@]2(C=O)C(OO)C(OO)C(OO)[C@@H]1OO2	0.22	1.24	2.29	4.0	0.71	1.00
15	$C_9H_{12}ClNO_7$	C[C@]1(C(C)(OO)C=C2)[C@H](Cl)[C@@]2(OO1)CO[N+]([O-])=O	0.17	1.97	2.36	4.0	0.92	0.72
16	$C_7H_8ClNO_7$	Cl[C@@H]([C@@H]1C(OO)C=C2)[C@@]2(OO1)CO[N+]([O-])=O	0.17	1.79	2.14	4.0	0.77	0.46
17	$C_{10}H_8$	C12=CC=CC=C1C=CC=C2	0.50	2.39	2.42	4.0	0.32	0.00

***** The class levels follow the guidelines of the Globally Harmonized System of Classification and Labelling of Chemicals (GHS). class 1 (highest hazard): pLD50 ≥ 4.3; class 2: 4.3> pLD50 >3.3; class 3: 3.3> pLD50 >2.5; class 4: 2.5> pLD50 >1.69; class 5(likely hazard): 1.69> pLD50 >1.3. (Europe, 2021)

****** class 1 (highest hazard): > 0.5; class 2 (likely hazard): ≤ 0.5. (Europe, 2021)

Table S6. Reaction mechanisms were used to model the fate of RO_2 generated from Cl-initiated oxidation of m-xylene in the absence of H_2O and NOx in the flow tube (Exp.1 in Table 1). The number in front of the product indicates the yield of the products.

Reactant 1	Reactant 2	Product 1	Product 2	Product 3	Rate Coeff.	Citation
Cl_2		2Cl			1.88E-19 $flux_{350nm}$	(DeMore et al., 1997)
m-xylene	Cl	0.5 RO_2	0.5 others	HCl	1.35E-10	(Wang et al., 2005)
RO_2	RO_2	RO	0.5ROH	0.5RCOR	1.30E-12	(Berndt et al., 2017)
RO_2		$R'O_2$			0.008	(Fu et al., 2020)
RO_2	Cl	RO	ClO		1.60E-10	(DeMore et al., 1997)
RO_2	ClO	RO	ClO_2		2.25E-12	(DeMore et al., 1997)
RO		$ROHRO_2$	RO_2		1.10E6	(Fu et al., 2020)
$R'O_2$	Cl	RO_2			1.60E-10	
$R'O_2$	ClO	RO_2			2.25E-12	
$R'O_2$	RO_2	R'O	0.5ROH	0.5RCOR	1.30E-12	(Berndt et al., 2017)
$R'O_2$	$R'O_2$	R'O	0.5R'OH	0.5R'COR	1.30E-12	(Berndt et al., 2017)
ROH	Cl	RO_2			1.80E-10	
RCOR	Cl	RO_2			1.80E-10	

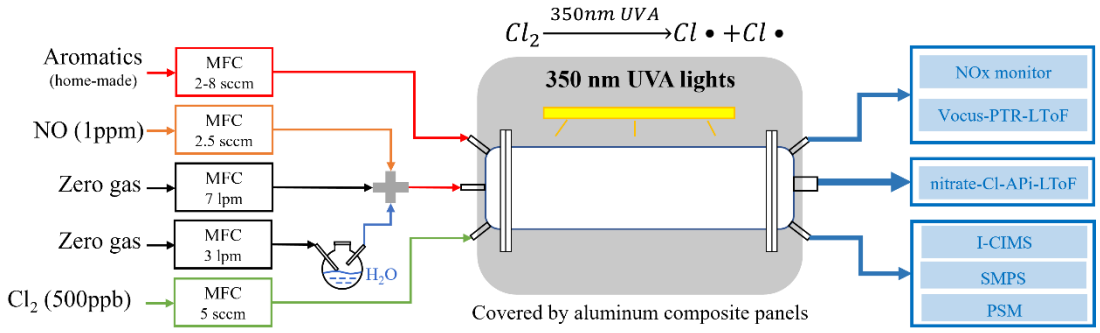

Figure S1. A scheme of the flow tube set-up and instruments used in the laboratory experiments. MFC: mass flow controller; SCCM: Standard Cubic Centimeters per Minute; LPM: Liters per Minute. Humidity, Cl_2, NO, and precursor flow rates were dynamically adjusted in response to feedback from back-end detectors. A SMPS (Scanning Mobility Particle Sizer with a nano Differential Mobility Analyzer, TSI, USA) was used to measure 4-60 nm particles, and a PSM (A10 particle size magnifier with CPC, Airmodus, Finland) was used to detect the sub-3 nm particles. No particles were observed during all experiments. Throughout the entire experiment, all detection equipment continuously monitors the precursor and products in real time. To minimize potential spatial discrepancies, care was taken to ensure consistent sampling across instruments. In our flow tube system (120 cm length, 8 cm internal diameter), the nitrate-CI-APi-LToF samples from the center of the flow tube, while other instruments (e.g., Vocus-PTR-LToF, I-CIMS, NOx monitor, SMPS, and PSM) sample from side ports positioned 4 cm off-center—i.e., halfway across the tube radius. Under the typical laminar flow conditions in our system (Reynolds number $\approx$ 200) and a residence time of ~36 s, radial diffusion is sufficient to promote near-uniform mixing across the tube cross-section. Furthermore, the side sampling ports are directed toward the centerline to minimize radial bias. Based on the geometry and previous test comparisons, the differences in concentration between sampling positions were determined to be negligible.

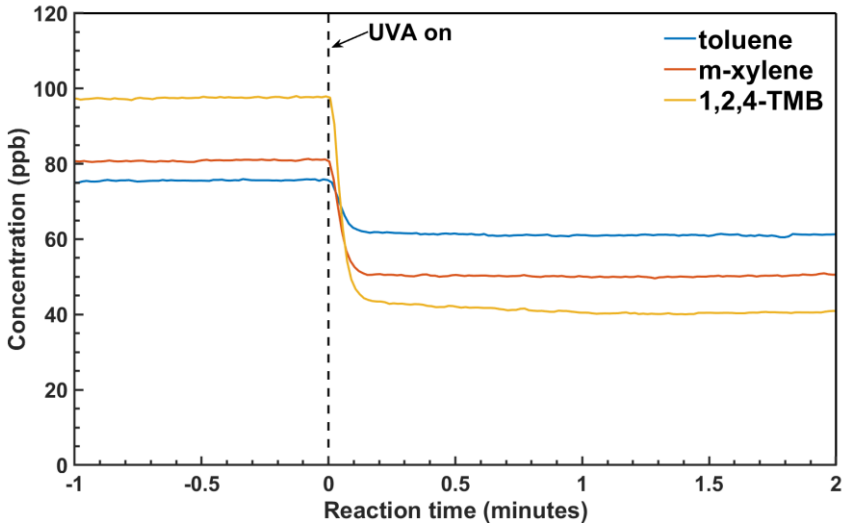

Figure S2. Real-time concentration of aromatic precursors (toluene, m-xylene, and 1,2,4-trimethylbenzene) measured by Vocus-PTR-LToF during the Cl-initiated oxidation experiment (refer to Exp. 1,5, and 9 in Table 1). The black dashed line at t = 0 marks the onset of UVA, which initiates the photolysis of Cl_2 and the subsequent formation of Cl radicals.

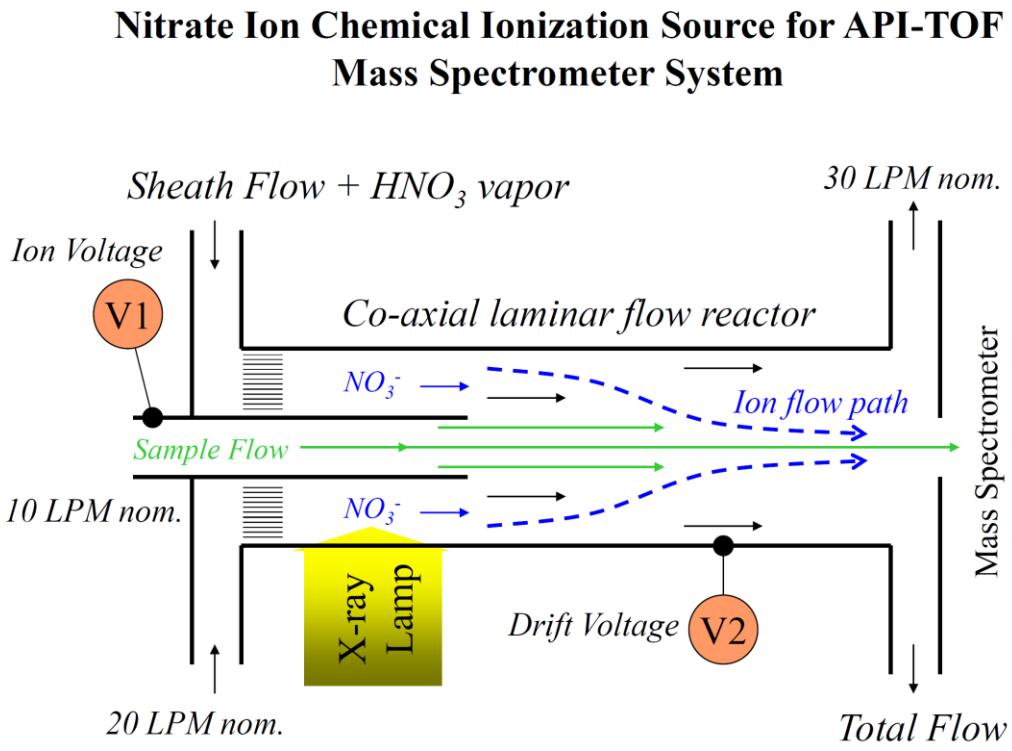

Figure S3. Schematic diagram of the nitrate-CI inlet (The image is provided by Aerodyne Research Inc.). While the detection of highly oxygenated organic molecules by nitrate-CI-APi-LToF is well-established, the identification of species with only one or two oxygen atoms (e.g., $C_8H_{12}Cl_2O$ or $C_2H_2Cl_2O_2$) involves greater uncertainty due to lower ionization efficiency. Nevertheless, previous studies have shown that nitrate-CI-APi-LToF can detect some moderately oxygenated compounds if they contain functional groups with sufficient gas-phase acidity or hydrogen bonding capacity (e.g., hydroxyl, carboxyl, or halogen substituents), which enhance clustering efficiency (Bianchi et al., 2019; Ehn et al., 2014).

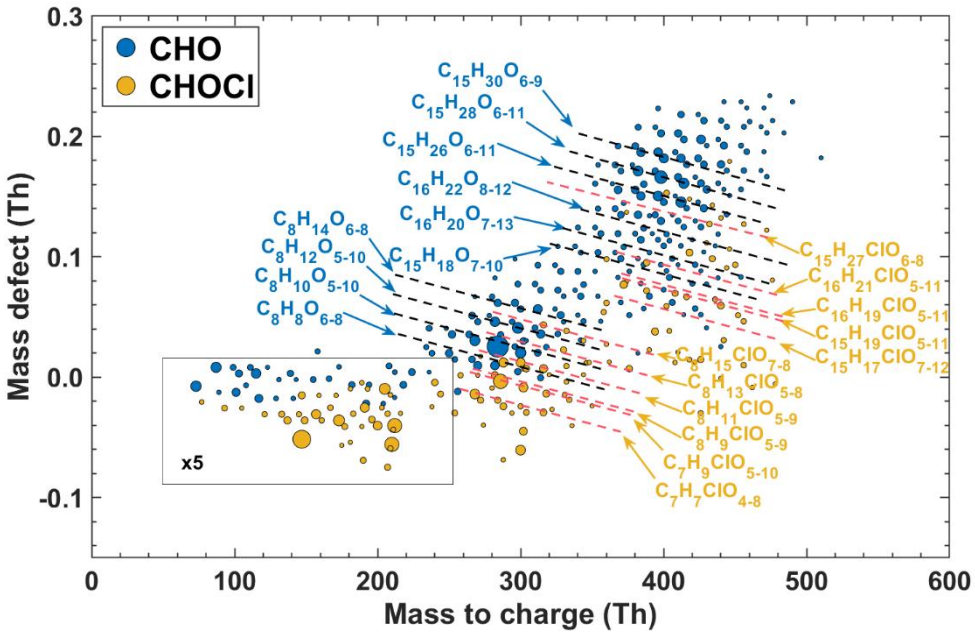

Figure S4. Mass defect plots of OOM products detected by a nitrate-CI-APi-LTOF from Cl-initiated reaction of m-xylene at 68% RH. The detected products are marked by their exact mass (with NO_3^- reagent ions) and mass defect (exact mass subtracted by its unit mass). The lines annotate the general chemical formulae. Cl-containing and non-Cl-containing formulae are shown in different colors. The size of the circle corresponds to the concentration of products.

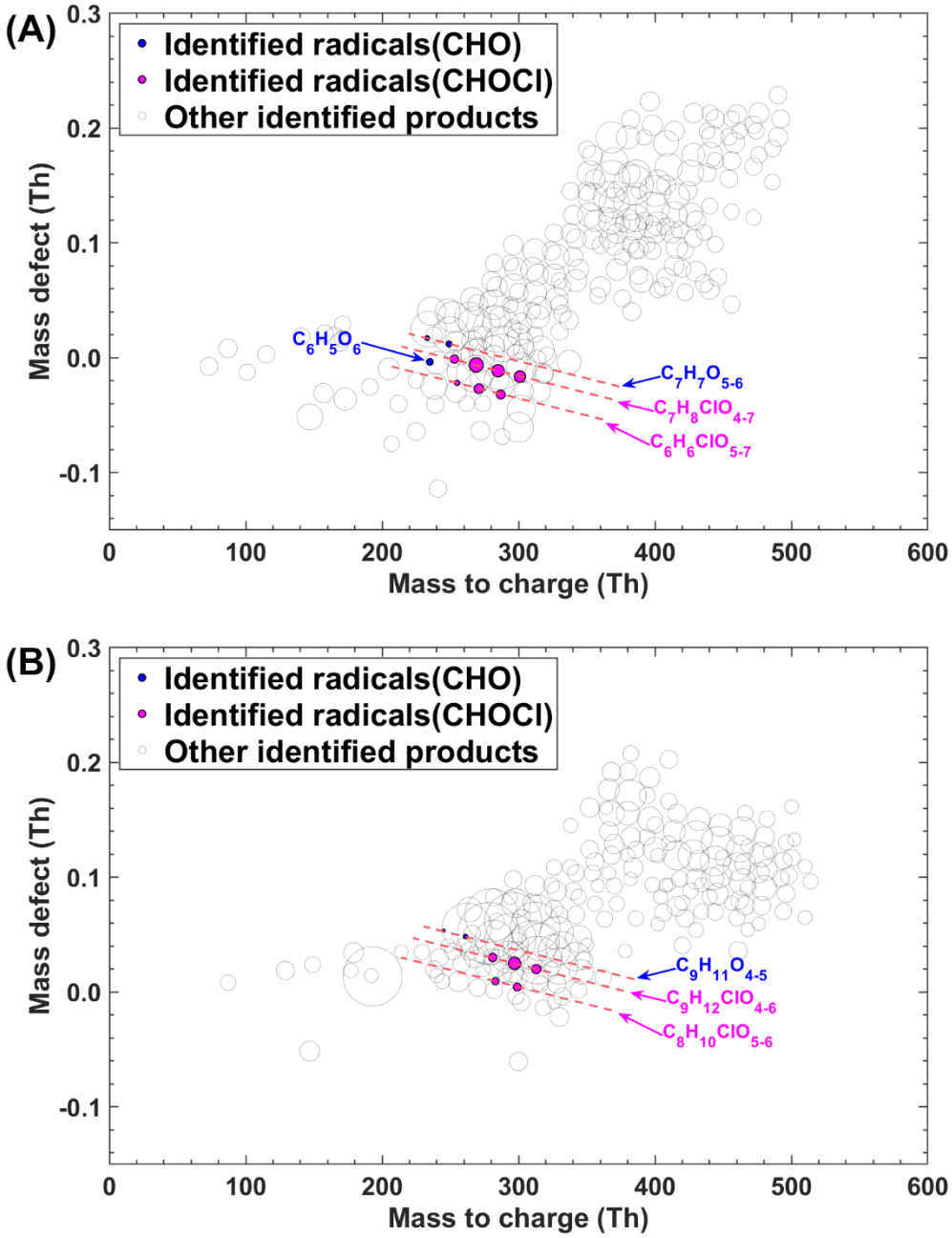

Figure S5. Mass defect plot of peroxyl radicals detected by nitrate-CI-APi-LTOF from Cl-initiated reaction of toluene (A) and 1,2,4-trimethylbenzene (B) without NO_x. The detected products and intermediate radicals are marked in the mass defect plot by their exact mass (with NO_3^- reagent ions) and mass defect (exact mass subtracted by its unit mass). The lines annotate the general chemical formulas. Chlorine-containing and non-chlorine-containing formulas are shown in different colors. The size of the circle is proportional to the five times concentration of peroxyl radicals.

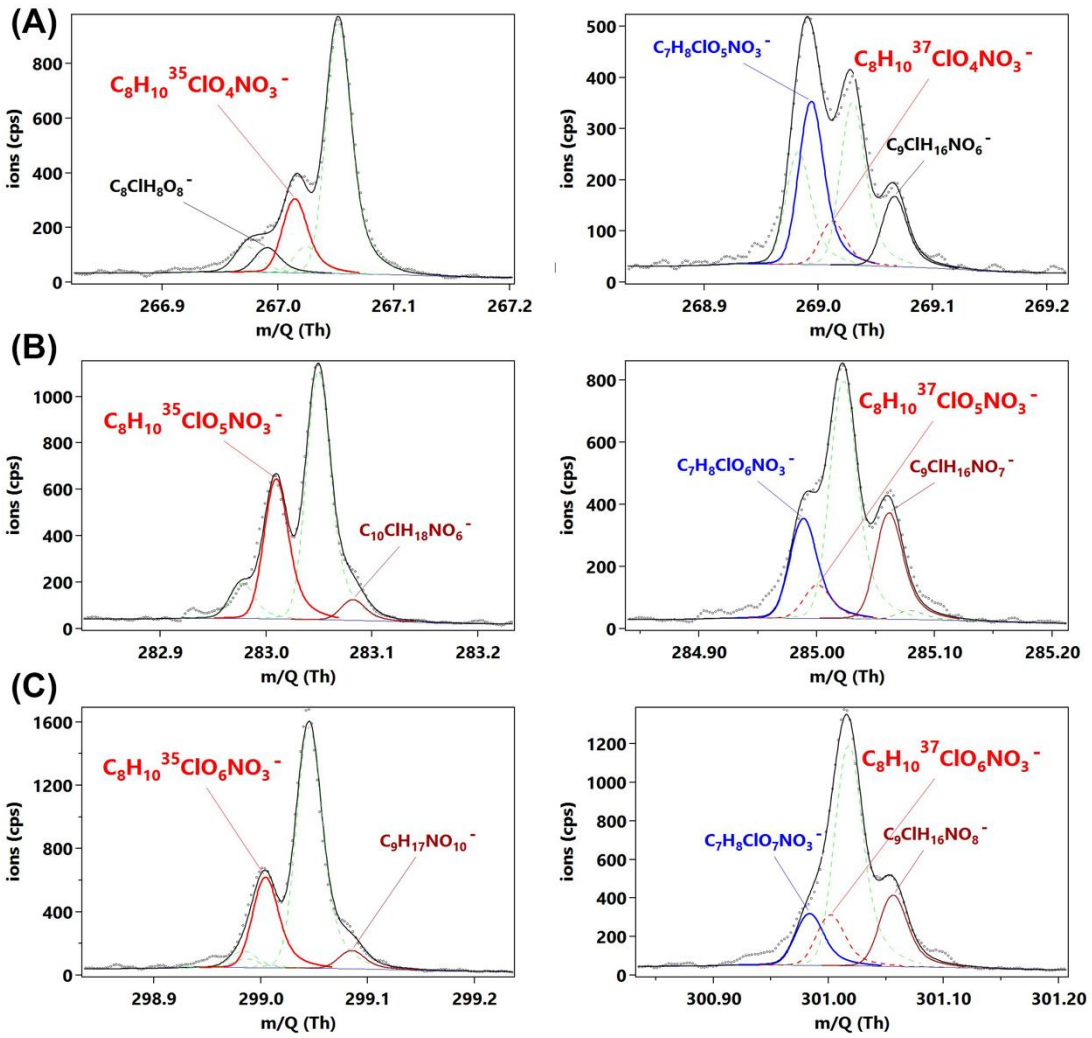

Figure S6. High-resolution peak fittings of selected Cl-containing radicals and their isotope peaks detected by nitrate CI-APi-LToF in m-Xylene + Cl reactions under NOx-free conditions (A) $C_8H_{10}{}^{35}ClO_4NO_3^-$ (left) and $C_8H_{10}{}^{37}ClO_4NO_3^-$ (right), (B) $C_8H_{10}{}^{35}ClO_5NO_3^-$ (left) and $C_8H_{10}{}^{37}ClO_5NO_3^-$ (right), (C) $C_8H_{10}{}^{35}ClO_6NO_3^-$ (left) and $C_8H_{10}{}^{37}ClO_6NO_3^-$ (right). The Cl-containing isotope peak is delineated by the red dashed line.

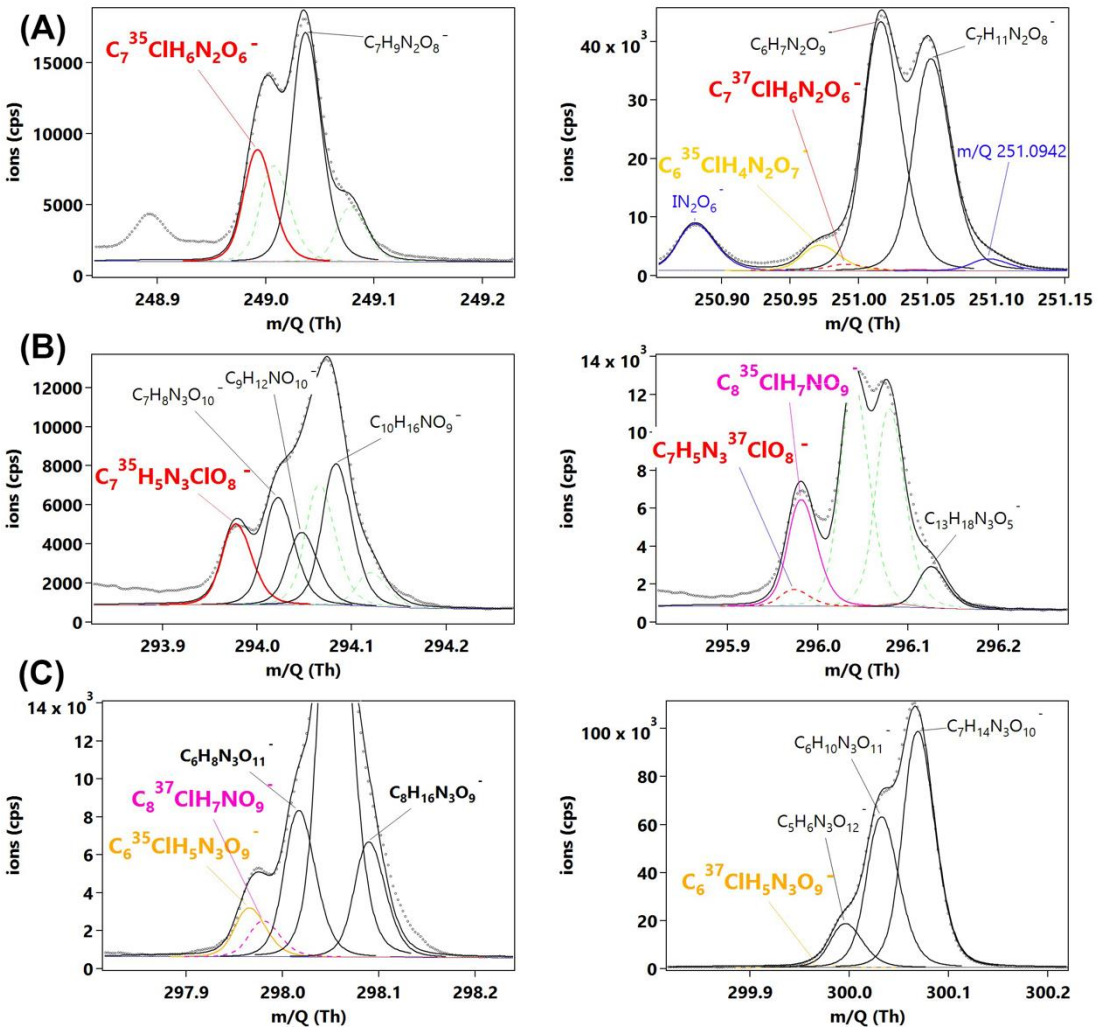

Figure S7-(1). High-resolution peak fittings of selected Cl-OOMs, (A) $C_7H_6{}^{35}ClNO_3NO_3^-$ (left) and $C_7H_6{}^{37}ClNO_3NO_3^-$ (right), (B) $C_7H_5{}^{35}ClN_2O_5NO_3^-$ (left) and $C_7H_5{}^{37}ClN_2O_5NO_3^-$ (right), (C) $C_6H_5{}^{35}ClN_2O_6NO_3^-$ (left) and $C_6H_5{}^{37}ClN_2O_6NO_3^-$ (right), based on two-hour averaged mass spectrum of nitrate CI-APi-LToF between 9:30-11:30 on January 17th, 2023, at the Dianshan Lake Air Quality Monitoring Supersite in Shanghai, China.

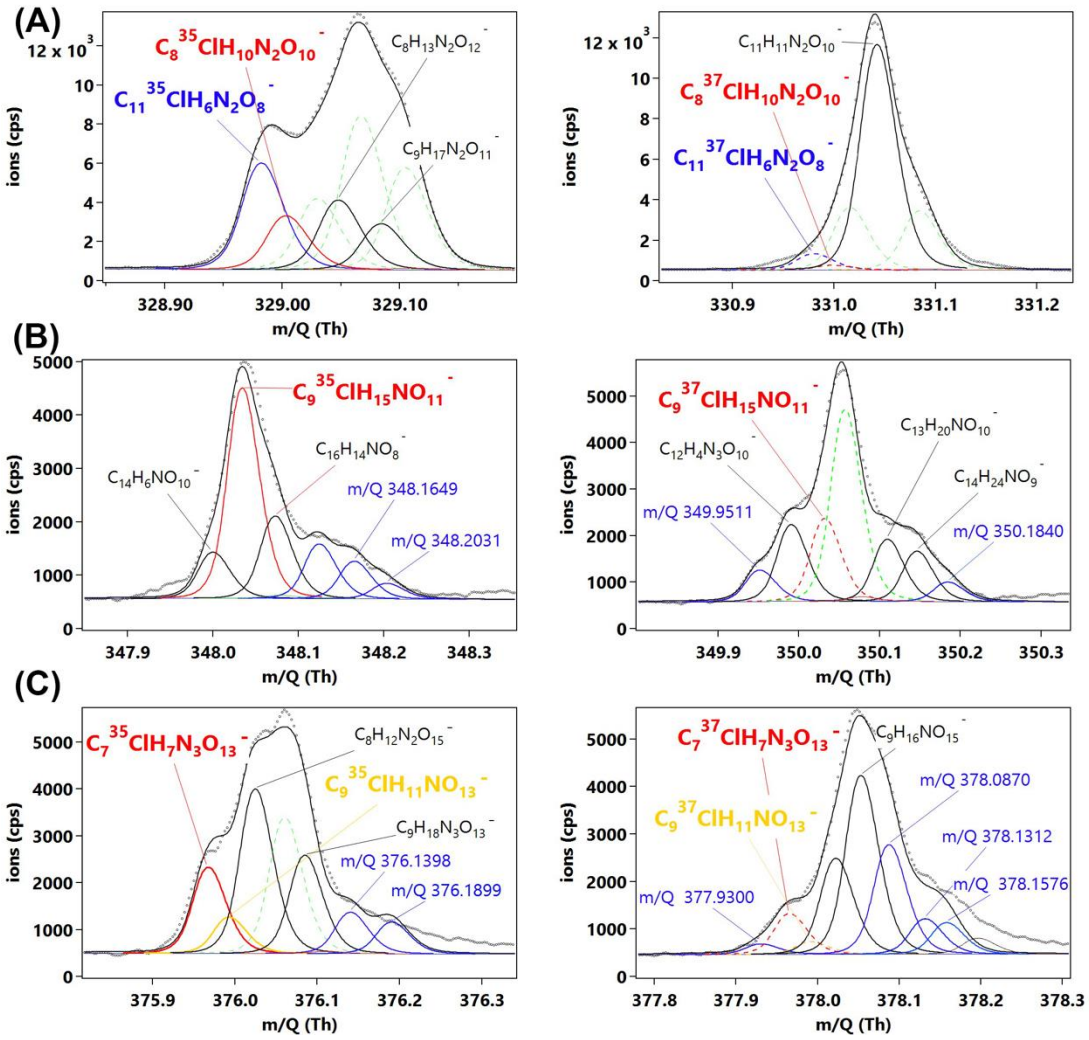

Figure S7-(2). Continued high-resolution peak fittings of selected Cl-OOMs, (A) $C_8H_{10}{}^{35}ClNO_7NO_3^-$ (left) and $C_8H_{10}{}^{37}ClNO_7NO_3^-$ (right), (B) $C_9H_{15}{}^{35}ClO_8NO_3^-$ (left) and $C_9H_{15}{}^{37}ClO_8NO_3^-$ (right), (C) $C_7H_7{}^{35}ClN_2O_{10}NO_3^-$ (left) and $C_7H_7{}^{37}ClN_2O_{10}NO_3^-$ (right), based on two-hour averaged mass spectrum of nitrate CI-APi-LToF between 9:30-11:30 on January 17th, 2023, at the Dianshan Lake Air Quality Monitoring Supersite in Shanghai, China.

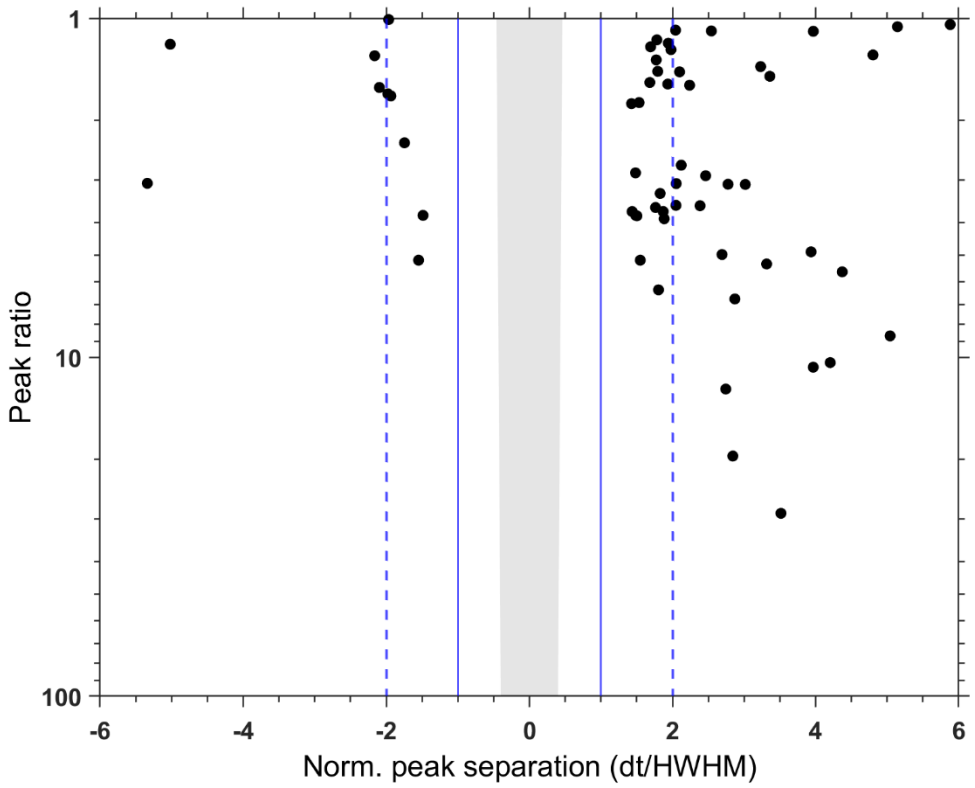

Figure S8. The ratio of the fitted peak intensities to the peak separation of all identified Cl-OOM peaks and adjacent ions from nitrate-Cl-APi-LToF data in field measurement. (Peak ratio: Ratio of parent-to-child intensities for an overlapping ion pair; dt: Separation of the known peak positions in time-of-flight space; HWHM: half-widths at half-maximum). It is noted that the region for dt/HWHM < 0.4 is shown in grey and is often considered to be two peaks that cannot be separated.

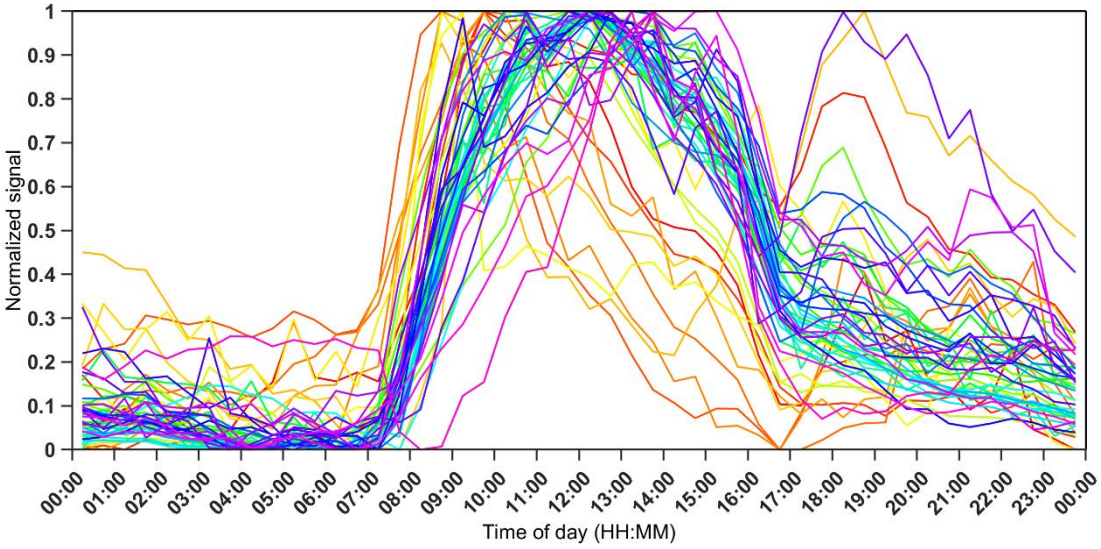

Figure S9. Mean diurnal profiles of all 51 Cl-OOMs detected by nitrate-CI-APi-LToF from December 14th, 2022, to February 2nd, 2023. The molecular formulas of the OOMs are presented in Table S3.

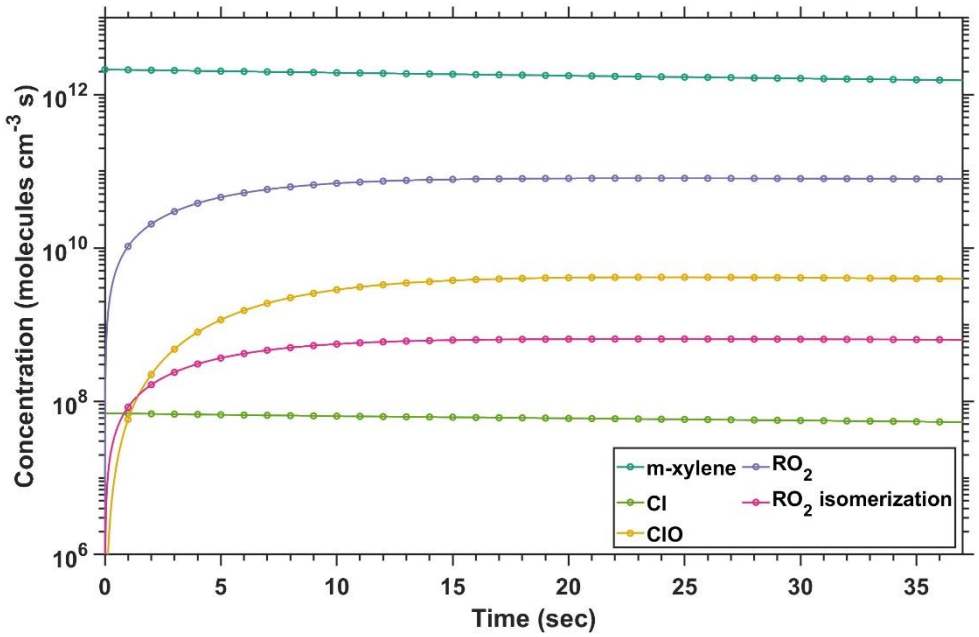

Figure S10. Time series of concentrations of m-xylene, Cl, ClO, RO_2, and RO_2 isomerization in the Cl + m-xylene experiment (Exp.1 in Table 1), as simulated by the PAM chemistry model.

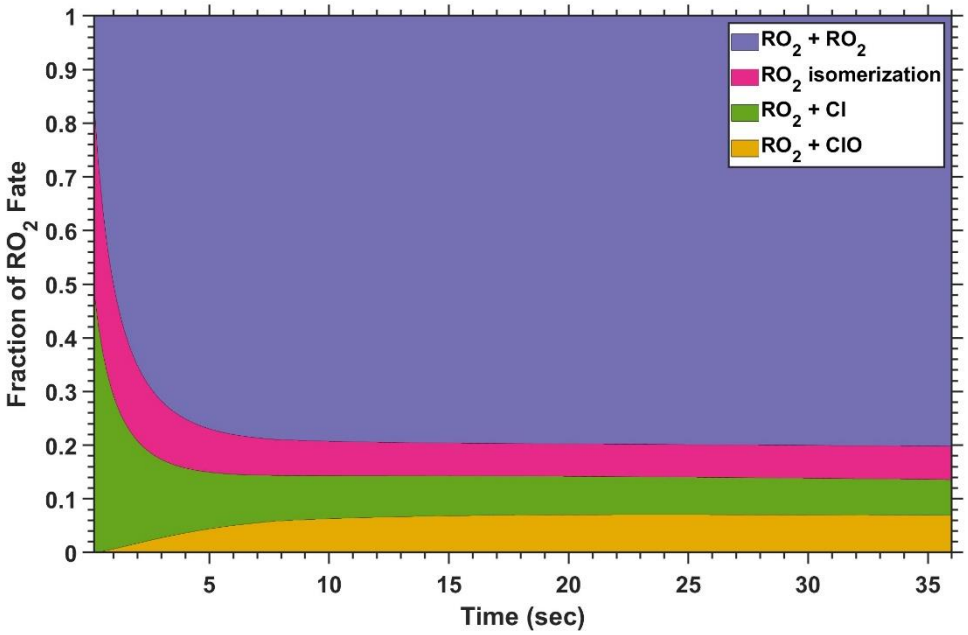

Figure S11. The fate of organic peroxy radicals (RO_2) generated from Cl (dry) oxidation of m-xylene (Exp.1 in Table 1) as a function of reaction time.

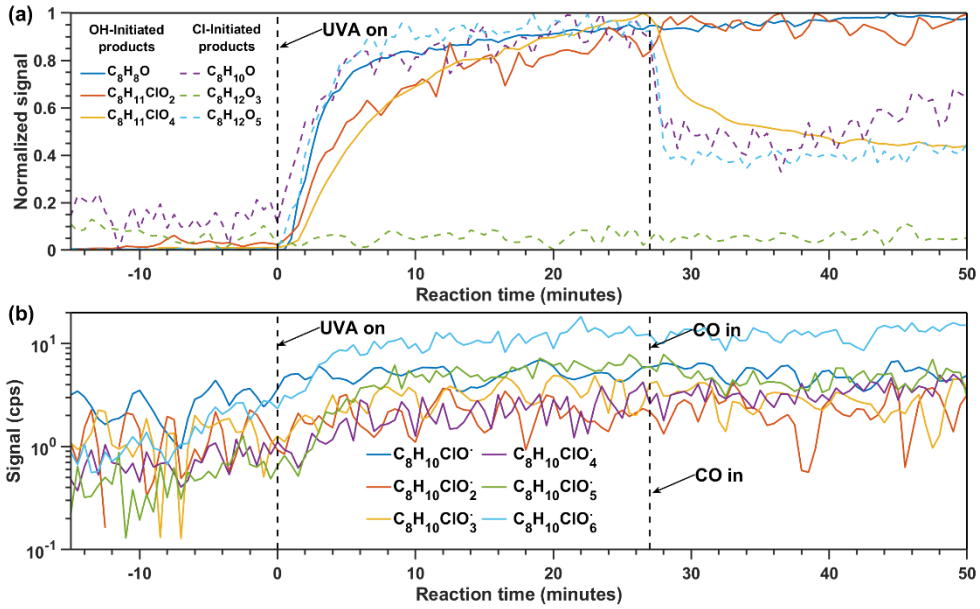

Figure S12. Time-resolved signal intensities of radicals and selected first-generation products from the Cl + m-xylene reaction in the absence of NOx. (a) Normalized signals of representative first-generation products, categorized by their dominant formation pathway (Cl-initiated vs. OH-initiated). C_8H_8O and $C_8H_{10}O$ were detected by Vocus-PTR-LToF; $C_8H_{11}ClO_2$, $C_8H_{11}ClO_4$, and $C_8H_{12}O_3$ were detected by I-CIMS; $C_8H_{12}O_5$ was detected by nitrate-CI-APi-LToF. (a) Absolute signals of the $C_8H_{10}ClO_{1\text{-}3}$ radical detected by nitrate-CI-APi-LToF and the $C_8H_{10}ClO_{4\text{-}6}$ radical detected by I-CIMS. The vertical dashed lines indicate the time points when UVA light was turned on (t = 0 min) and when CO was introduced (t ≈ 27 min) to terminate OH reactions.

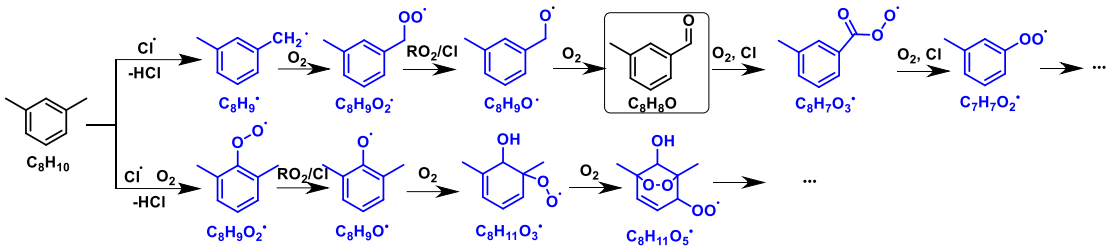

Scheme S1. Proposed reaction pathways for the formation of non-chlorinated oxygenated organic molecules (non-Cl-OOMs) from the Cl-initiated oxidation of m-xylene. The scheme illustrates two primary mechanisms: (1) hydrogen abstraction by Cl atoms from the methyl substituents, followed by O_2 addition and autoxidation; and (2) hydrogen abstraction from aromatic positions (less favorable), also followed by autoxidation. Both pathways can lead to the formation of a range of non-Cl-containing RO_2 radicals and closed-shell products. Representative detected or inferred molecular formulas are labeled in blue.

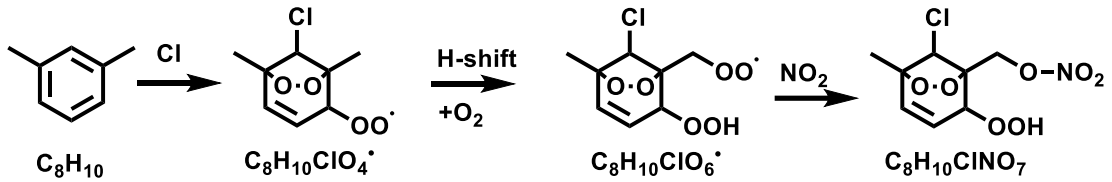

Scheme S2. Formation mechanisms of $C_8H_{12}ClNO_8$ in reactions of Cl and m-xylene involving only Cl.

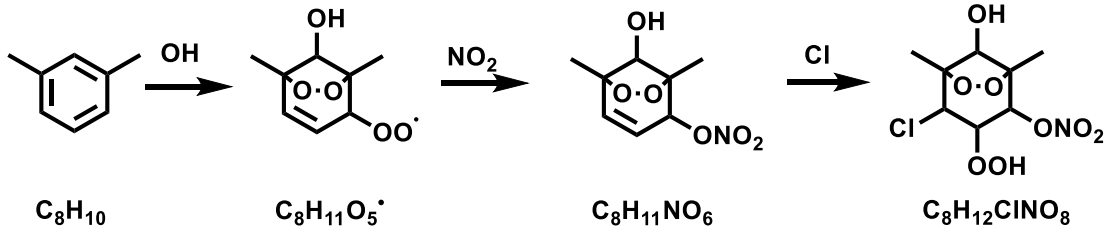

Scheme S3. Formation mechanisms of $C_8H_{12}ClNO_8$ in reactions of Cl and m-xylene involving both OH and Cl.

References

Baker, Y., Kang, S., Wang, H., Wu, R., Xu, J., Zanders, A., He, Q., Hohaus, T., Ziehm, T., Geretti, V., Bannan, T. J., O'Meara, S. P., Voliotis, A., Hallquist, M., McFiggans, G., Zorn, S. R., Wahner, A., and Mentel, T. F.: Impact of HO2/RO2 ratio on highly oxygenated α-pinene photooxidation products and secondary organic aerosol formation potential, Atmos. Chem. Phys., 24, 4789–4807, https://doi.org/10.5194/acp-24-4789-2024, 2024.

Berndt, T., Scholz, W., Mentler, B., Fischer, L., Herrmann, H., Kulmala, M., and Hansel, A.: Accretion Product Formation from Self- and Cross-Reactions of RO2 Radicals in the Atmosphere., Angewandte Chemie Int Ed Engl, 57, 3820–3824, https://doi.org/10.1002/anie.201710989, 2017.

Bhattacharyya, N., Modi, M., Jahn, L. G., and Ruiz, L. H.: Different chlorine and hydroxyl radical environments impact m -xylene oxidation products, Environ. Sci.: Atmos., https://doi.org/10.1039/d3ea00024a, 2023.

Bianchi, F., Kurtén, T., Riva, M., Mohr, C., Rissanen, M. P., Roldin, P., Berndt, T., Crounse, J. D., Wennberg, P. O., Mentel, T. F., Wildt, J., Junninen, H., Jokinen, T., Kulmala, M., Worsnop, D. R., Thornton, J. A., Donahue, N., Kjaergaard, H. G., and Ehn, M.: Highly Oxygenated Organic Molecules (HOM) from Gas-Phase Autoxidation Involving Peroxy Radicals: A Key Contributor to Atmospheric Aerosol, Chem Rev, 119, 3472–3509, https://doi.org/10.1021/acs.chemrev.8b00395, 2019.

Ehn, M., Thornton, J. A., Kleist, E., Sipilä, M., Junninen, H., Pullinen, I., Springer, M., Rubach, F., Tillmann, R., Lee, B., Lopez-Hilfiker, F., Andres, S., Acir, I.-H., Rissanen, M., Jokinen, T., Schobesberger, S., Kangasluoma, J., Kontkanen, J., Nieminen, T., Kurtén, T., Nielsen, L. B., Jørgensen, S., Kjaergaard, H. G., Canagaratna, M., Maso, M. D., Berndt, T., Petäjä, T., Wahner, A., Kerminen, V.-M., Kulmala, M., Worsnop, D. R., Wildt, J., and Mentel, T. F.: A large source of low-volatility secondary organic aerosol, Nature, 506, 476–479, https://doi.org/10.1038/nature13032, 2014.

DeMore, W. B., Sander, N. P., Golden, D. M., Hampson, R. F., Kurylo, M. J., Howard, C. J., Ravishankara, A. R., Kolb, C. E., and Molina, M. J.: Chemical Kinetics and Photochemical Data for Use in Stratospheric Modeling, JPL Publication, 1997.

Europe, U. N. E. C. for: Globally Harmonized System of Classification and Labelling of Chemicals (GHS), Glob. Harmon. Syst. Classif. Label. Chem. (GHS), https://doi.org/10.18356/9789210052139, 2021.

Fu, Z., Xie, H.-B., Elm, J., Guo, X., Fu, Z., and Chen, J.: Formation of Low-Volatile Products and Unexpected High Formaldehyde Yield from the Atmospheric Oxidation

of Methylsiloxanes, Environ. Sci. Technol., 54, 7136–7145, https://doi.org/10.1021/acs.est.0c01090, 2020.

Huang, M., Wang, Z., Hao, L., and Zhang, W.: DFT study on the abstraction and addition of Cl atom with toluene, Comput. Theor. Chem., 996, 44–50, https://doi.org/10.1016/j.comptc.2012.07.011, 2012.

Jahn, L. G., McPherson, K. N., and Ruiz, L. H.: Effects of Relative Humidity and Photoaging on the Formation, Composition, and Aging of Ethylbenzene SOA: Insights from Chamber Experiments on Chlorine Radical-Initiated Oxidation of Ethylbenzene, ACS Earth Space Chem., 8, 675–688, https://doi.org/10.1021/acsearthspacechem.3c00279, 2024.

Keller-Rudek, H., Moortgat, G. K., Sander, R., and Sörensen, R.: The MPI-Mainz UV/VIS Spectral Atlas of Gaseous Molecules of Atmospheric Interest, Earth Syst. Sci. Data, 5, 365–373, https://doi.org/10.5194/essd-5-365-2013, 2013.

Kürten, A., Rondo, L., Ehrhart, S., and Curtius, J.: Calibration of a Chemical Ionization Mass Spectrometer for the Measurement of Gaseous Sulfuric Acid, J Phys Chem, 116, 6375–6386, https://doi.org/10.1021/jp212123n, 2012.

Peng, Z. and Jimenez, J. L.: Radical chemistry in oxidation flow reactors for atmospheric chemistry research, Chem Soc Rev, 49, 2570–2616, https://doi.org/10.1039/c9cs00766k, 2020.

Peng, Z., Day, D. A., Ortega, A. M., Palm, B. B., Hu, W., Stark, H., Li, R., Tsigaridis, K., Brune, W. H., and Jimenez, J. L.: Non-OH chemistry in oxidation flow reactors for the study of atmospheric chemistry systematically examined by modeling, Atmos. Chem. Phys., 16, 4283–4305, https://doi.org/10.5194/acp-16-4283-2016, 2016.

Platz, J., Nielsen, O. J., Wallington, T. J., Ball, J. C., Hurley, M. D., Straccia, A. M., Schneider, W. F., and Sehested, J.: Atmospheric Chemistry of the Phenoxy Radical, C6H5O(•): UV Spectrum and Kinetics of Its Reaction with NO, NO2, and O2, J. Phys. Chem. A, 102, 7964–7974, https://doi.org/10.1021/jp982221l, 1998.

Wang, L., Arey, J., and Atkinson, R.: Reactions of Chlorine Atoms with a Series of Aromatic Hydrocarbons, Environ Sci Technol, 39, 5302–5310, https://doi.org/10.1021/es0479437, 2005.

Wang, Y., Li, C., Zhang, Y., Li, Y., Yang, G., Yang, X., Wu, Y., Yao, L., Zhang, H., and Wang, L.: Secondary reactions of aromatics-derived oxygenated organic molecules lead to plentiful highly oxygenated organic molecules within an intraday OH exposure, Atmos. Chem. Phys., 24, 7961–7981, https://doi.org/10.5194/acp-24-7961-2024, 2024.